Redox Biology 36 (2020) 101592

Contents lists available at ScienceDirect

Redox Biology

journal homepage: www.elsevier.com/locate/redox

Reactive species generated by heme impair alveolar epithelial sodium channel function in acute respiratory distress syndrome

Saurabh Aggarwal[a,b,c,1], Ahmed Lazrak[a,b,c,1], Israr Ahmad[a,c], Zhihong Yu[a,b,c], Ayesha Bryant[a,c], James A. Mobley[a,b,c], David A. Ford[d], Sadis Matalon[a,b,c,*]

[a] Division of Molecular and Translational Biomedicine, USA
[b] Pulmonary Injury and Repair Center, USA
[c] Department of Anesthesiology and Perioperative Medicine, School of Medicine, University of Alabama at Birmingham, Birmingham, AL, 35205-3703, USA
[d] Department of Biochemistry and Molecular Biology, St. Louis University, St. Louis, MO, 63104, USA

ARTICLE INFO

Keywords:
Cell-free heme
Halogenated lipids
Carbonylation
Hemopexin
Spectrin
Epithelial sodium channel

ABSTRACT

We previously reported that the highly reactive cell-free heme (CFH) is increased in the plasma of patients with chronic lung injury and causes pulmonary edema in animal model of acute respiratory distress syndrome (ARDS) post inhalation of halogen gas. However, the mechanisms by which CFH causes pulmonary edema are unclear. Herein we report for the first time that CFH and chlorinated lipids (formed by the interaction of halogen gas, Cl_2, with plasmalogens) are increased in the plasma of patients exposed to Cl_2 gas. *Ex vivo* incubation of red blood cells (RBC) with halogenated lipids caused oxidative damage to RBC cytoskeletal protein spectrin, resulting in hemolysis and release of CFH. Patch clamp and short circuit current measurements revealed that CFH inhibited the activity of amiloride-sensitive epithelial Na^+ channel (ENaC) and cation sodium (Na^+) channels in mouse alveolar cells and trans-epithelial Na^+ transport across human airway cells with EC_{50} of 125 nM and 500 nM, respectively. Molecular modeling identified 22 putative heme-docking sites on ENaC (energy of binding range: 86–1563 kJ/mol) with at least 2 sites within its narrow transmembrane pore, potentially capable of blocking Na^+ transport across the channel. A single intramuscular injection of the heme-scavenging protein, hemopexin (4 μg/kg body weight), one hour post halogen gas exposure, decreased plasma CFH and improved lung ENaC activity in mice. In conclusion, results suggested that CFH mediated inhibition of ENaC activity may be responsible for pulmonary edema post inhalation injury.

1. Introduction

In this study we found that patients exposed to Cl_2 gas during an industrial accident in 2019 at a water treatment facility in Birmingham, Alabama, US, had elevated plasma levels of cell-free heme (CFH). Heme is an essential functional group of many proteins. However, non-encapsulated cell-free heme (CFH), a breakdown component of proteins such as hemoglobin, myoglobin, horseradish peroxidase, cytochrome b_5, and cytochrome P450 can cause oxidative damage and impair cellular integrity [1] and is implicated in the pathogenesis of several disorders [2–10]. CFH is an abundant source of redox-active iron capable of damaging lipid, protein, and DNA [11–13]. In addition, CFH intercalates into cell membranes and disrupts plasma membrane integrity [14]. Under normal conditions, circulating CFH is maintained at low levels [15] by serum albumin and hemopexin [16–19].

In a recent publication, Shaver et al. found that cell-free hemoglobin levels in the air space correlated with alveolar-capillary barrier dysfunction in humans with acute respiratory distress syndrome (ARDS) [20]. Further, they demonstrated that the intratracheal administration of cell-free hemoglobin to mice resulted in alveolar-capillary barrier disruption and acute lung injury [20]. Interestingly, they also found that the effects of cell-free hemoglobin were mediated by the iron-containing heme moiety of cell-free hemoglobin, as intratracheal administration of CFH was sufficient to increase alveolar permeability in mice [20]. In fact in our recent studies, we found that patients with chronic obstructive pulmonary disease (COPD) also had elevated levels of CFH [8] which correlated with the severity of the disease. In an animal model of ARDS, we found that scavenging CFH reduced pulmonary edema and improved lung function by attenuating the inflammatory cytokines and oxidative damage in the lungs suggesting

* Corresponding author. BMR II 224, 901 19th Street South, Birmingham, AL, 35205-3703, USA.
E-mail address: smatalon@uabmc.edu (S. Matalon).
[1] Authors contributed equally.

https://doi.org/10.1016/j.redox.2020.101592
Received 25 March 2020; Received in revised form 8 May 2020; Accepted 20 May 2020
Available online 01 June 2020

that CFH is involved in impairing endothelial barrier function [9]. Whether, CFH is also involved in impairing active alveolar fluid clearance in ARDS is unclear.

The amiloride-sensitive epithelial Na^+ channel (ENaC), an apical membrane protein complex, is the first and limiting step in Na^+ transport across the alveolar space of humans and animals. This process is driven by the energy consuming Na^+/K^+-ATPase (sodium–potassium adenosine triphosphatase) located in the basolateral side of epithelial cells and plays a critical role in fluid reabsorption especially when the alveolar epithelium is damaged and permeability to plasma proteins is increased [21]. Most important, this process of alveolar fluid clearance is impaired in ARDS [22]. Ware et al. measured net alveolar fluid clearance in 79 patients with acute lung injury or ARDS and found that 56% had impaired alveolar fluid clearance, and 32% had submaximal clearance and only 13% had maximal clearance [22]. They also found that patients with maximal alveolar fluid clearance had significantly lower mortality and a shorter duration of mechanical ventilation [22]. A decline in Na^+ and fluid clearance has also been reported in animal models of lung injury and ARDS. Vivona et al. demonstrated that hypoxia reduced Na^+ conductance by attenuating ENaC activity [23]. Polyubiquitination and decrease in cell surface stability of ENaC due to hypercapnia was reported by Gwozdzinska et al. as an important cause of decline in vectorial transport of Na^+ across alveolar epithelium in an animal model of ARDS [24]. Here, we explored whether CFH is responsible for ENaC impairment in an animal model of ARDS.

We developed an animal model of ARDS by exposing C57BL/6 mice to halogen gases such as chlorine (Cl_2) or bromine (Br_2). We have previously shown that exposure to Br_2 (600 ppm, 30min) or Cl_2 (400 ppm, 30min) causes lung pathology similar to ARDS [9,25–27] and that this injury is mediated at least in part by halogenated lipids, formed by the interaction of halogen gases with plasmalogens on the surface of lung epithelial cells, which are released into the alveolar spaces and plasma. Recent studies have shown that these halogenated lipids are elevated in patients who have ARDS [28] secondary to sepsis and also correlate with the disease severity [28].

Here, we report that halogenated lipids increased oxidation of red blood cell (RBC) structural protein, spectrin, thereby increasing RBC fragility and rupture. The resultant CFH impaired the activity of ENaC *in vitro* and *in vivo*. However, treating animals with the heme scavenging protein, hemeopexin, reduced RBC oxidation, hemolysis, and improved ENaC activity. Using molecular modeling, we also predicted potential heme binding sites on ENaC which may be used in future to develop additional therapeutic strategies to increase ENaC activity and reduce pulmonary edema post ARDS.

2. Methodology

Human: The study was approved by the University of Alabama at Birmingham Institutional Review Board (IRB Protocol 300002065 and 300000860) and the Saint Louis University Institutional Review Board (IRB 9952). Demographic information were recorded on all volunteers and blood was drawn from peripheral vein. Plasma was isolated from the blood, aliquoted, and stored at −80 °C using Freezerworks Sample Inventory Management software (Dataworks Development, Inc, Mountlake Terrace, WA, USA). No samples had undergone freeze-thaw cycles prior to use in the study.

Animals: Adult male C57BL/6 mice (20–25 g) were bought from Charles River, non-Frederick/NCI. All mice used in the study were males. All mice were raised under a 12-h dim light/12-h dark cycle with access to a standard diet and tap water ad libitum. Euthanasia protocol based on intraperitoneal injections of ketamine and xylazine was used in the study for mice to minimize pain and distress. All animal care and experimental procedures were approved by the Institutional Animal Care and Use Committee at the University of Alabama in Birmingham.

Exposure to halogen gas: Mice were exposed to Br_2 gas (600 ppm) or Cl_2 gas (400 ppm) in a cylindrical glass chamber for 30 min, as previously described [9,26]. Control mice were exposed to room air in the same experimental conditions as Br_2 or Cl_2 exposed mice. Exposures were performed with two mice in the same chamber at any one time, and all exposures were performed between 6:00 a.m. and 12:00 p.m. Tanks were replaced when the pressure in the tanks reached 500 psi. In each case, immediately following exposure, mice were returned to room air. All experiments involving animals were conducted according to protocols approved by the UAB IACUC.

Treatment of animals with hemopexin: Adult male C57BL/6 mice were exposed to Br_2 gas (600 ppm), Cl_2 gas (400 ppm), or air in a cylindrical glass chamber for 30 min, as described above. Following exposure, mice were returned to room air and then 1 h later, mice were treated with an intramuscular injection of either saline or purified human hemopexin (4 mg/kg body weight, dissolved in saline) (Product No. 16-16-080513-LEL; Athens Research and Technology, Athens, GA). All experiments involving animals were conducted according to protocols approved by the UAB IACUC.

Measurement of Br-lip: Mice were euthanized at various times post-Br_2 gas exposure using a mixture of ketamine/xylazine (200/10 mg/kg) administered by intraperitoneal injection. Blood was collected via cardiac puncture, lungs were excised, and urine was collected from the bladder. Blood was centrifuged at 6000 rpm for 5 min to obtain the plasma fraction. Lungs, urine, and plasma samples were flash-frozen in liquid nitrogen and stored at −80 °C. In some mice, the lungs were lavaged, and the recovered bronchoalveolar lavage fluid (BALF) was centrifuged immediately at 3000 *g* for 10 min to pellet the cells. Supernatants were flash-frozen. All samples were shipped overnight on dry ice to Dr. Ford at St. Louis University. Br-FALD was measured following conversion to its pentafluorobenzyl oxime using negative ion-chemical ionization GC/MS as previously described [29]. Free, esterified, and total (free + esterified) Br-FA were measured as previously described for chlorine by LC/MS following Dole extraction [26,30]. Total lipids were measured by LC/MS after base hydrolysis and esterified Br-FA calculated by subtracting free lipids from total lipids. Extractions were performed using 25 μl of plasma spiked with 517 fmol of 2-chloro-[d_4-7,7,8,8] palmitic acid (2-[d_4]ClPA) as the internal standard, and for lungs, 40–50 mg of tissue was used, spiked with 20 pmol of 2-[d_4]ClPA internal standard as mentioned earlier for Cl–FAs [26].

Measurement of glutathione adducts of 2-Br-PALD: Plasma, lung, BALF, and urine samples were analyzed as previously described [26]. Briefly, 25 μl of plasma, RBCs (diluted with 75 μl of water), BALF or urine were spiked with 90 fmol of [d_4]HDAGSH and 10 mg of pulverized lung tissue was spiked with 900 fmol [d_4]HDAGSH. Plasma, lung, RBCs, BALF, and urine were then extracted according to a similar Bligh and Dyer method as described for the Cl-lipids [30]; however, the aqueous layer was saved as the GSH adducts partition to the aqueous layer. The organic layer was subsequently washed with 1 volume of methanol:water (1:1 v:v) and combined with the previous aqueous layer. The combined aqueous layers were diluted with 1/3 vol of water and extracted on a Strata-X followed by ESI-LC/MS/MS quantitation, as previously described [31].

***Ex Vivo* RBC mechanical fragility:** Blood was obtained from adult C57BL/6 mice in the presence of an anticoagulant and incubated with 1 μM each of Br-lip (16BrFA, 16BrFALD, 18BrFA, 18BrFALD), Cl-lip (16ClFA, 16ClFALD, 18ClFA, or 18ClFALD) or the corresponding non-halogenated lipids as vehicle (16 and 18 carbon palmitic acid or palmitaldehyde) for 4 h with rotations. In a separate set of experiments, blood was obtained from mice exposed to Br_2, Cl_2, or air in the presence or absence of treatment with hemopexin as mentioned above. Plasma was separated and the RBCs were washed with isotonic solution 3 times to remove traces of plasma. RBCs were then re-suspended in normal saline. The RBC suspensions along with 4 × 4mm glass beads (Pyrex) in DPBS were then rotated 360° for 2 h at 24 rpm at 37 °C. The RBC suspension was then centrifuged at 13,400 g for 4 min to separate the intact or damaged cells from the supernatant containing heme/

hemoglobin from the lysed cells during this mechanical stress. Free heme/hemoglobin was transferred into a new tube and the absorbance of the supernatant recorded at 540 nm as described earlier [32]. Subsequently, one hundred percent hemolysis of RBCs was achieved by treating them with 1% Triton x-100 solution. The fractional hemolysis of the sample was then obtained by dividing the optical density of the sample by the optical density of the 100% hemolyzed sample.

Measurement of protein carbonyl adducts in RBC ghosts: RBCs were separated from the plasma and hemolyzed with 20 mM hypotonic Hepes Buffer. The mixture was centrifuged at 14,000 g for 20 min and RBC pellet was dissolved in RIPA buffer (Thermo Fisher Scientific, MA). The protein was quantified by the BCA method and equal amounts of proteins (10 μg) were loaded into a 4–20% gradient gel and proteins were separated and stained with Amido Black (Sigma-Aldrich, St Louis, MS). The presence of protein carbonyl adducts in RBC ghosts were assessed using the Oxyblot protein oxidation detection kit (Product number: S7150, EMD Millipore, Billerica, MA), according to the manufacturer's protocol. Briefly, the carbonyl groups in the protein side chains were derivatized to 2,4-dinitrophenylhydrazone by reacting with 2,4-dinitrophenylhydrazine. Precisely, 10 μg of protein was used for each sample, and the 2,4-dinitrophenol-derivatized protein samples were separated by polyacrylamide gel electrophoresis, as described previously [9]. Polyvinylidene fluoride membranes were incubated for 1 h in the stock primary antibody (1:150 in 1% PBS/TBST buffer), and after washing, for 1 h in the stock secondary antibody (1:300 in % PBS/TBST buffer). Membranes were washed 3 × in TBST and visualized. The abundance of protein carbonylation was assessed by densitometry of each lane and normalization for each lane protein loading was done by SDS PAGE gel quantification.

Lung slices preparation: Eight-week-old C57BL/6 male mice (~20–25 g body weight) were purchased from The Jackson Laboratory (Bar Harbor, ME). Lung slices were prepared as previously described [33]. The right lower lobes were dissected, attached to tissue holder using cyanoacrylate adhesive gel, and sectioned into slices of 200 μm thick. The slices were transferred to a six-well plate containing Dulbecco's Modified Eagle's Medium without serum, supplemented with penicillin–streptomycin, and allowed to recover at 37 °C in a humidified environment of 95% air/5% CO_2 for 2–3 h.

ENaC single channel activity in AT2 cells *in situ:* A lung slice was transferred to the recording chamber on the stage of an upright Olympus microscope EX51WI (Olympus, Pittsburgh, PA). Single-channel activity in AT2 cells was recorded using the cell-attached mode of the patch clamp technique [34,35]. AT2 cells were identified by the presence of scattered green fluorescence after incubation with Lysotracker Green (catalogue number DND-26; Invitrogen, Eugene, OR).

Human bronchial epithelial cells isolation, culture, and short circuit currents recording: Human bronchiolar epithelial cells (HBECs) were provided by UAB CF Center upon request. Cells were isolated from human lungs not used for transplantation, HBECs were seeded onto permeable support and allowed to form confluent monolayers (3–4 weeks in culture). Tight monolayers were mounted in an Ussing chambers system and short circuit currents were monitored and recorded using an amplifier (physiologic instruments, San Diego, CA). Monolayers were bathed in Ringer solution bubbled with 95% air 5% Co_2. Hemin (ferric chloride heme, mentioned as heme throughout the text), dissolved in DMSO, was added to both sides of monolayers.

ENaC expression in Xenopus oocytes: Detailed description of these techniques has been previously reported [35]. In brief, oocytes isolated from *Xenopus laevis* frogs, were injected with cRNAs encoding for wild-type α, β, γ-hENaC (8.4 ng each), dissolved in 50 nl of RNase-free water per oocyte, and incubated in half-strength L-15 medium for 24–48 h. Whole-cell cation currents were measured by the two-electrode voltage clamp. A TEV 200 voltage clamp amplifier (Dagan Corp., Minneapolis, MN) was used hold oocytes membrane potential at −40 mV. Current–voltage (I–V) relationships were obtained by stepping the Vm from −140 mV to +60 mV in 20 mV increments. Sampling protocols were generated by pCLAMP 9.0 (Molecular Devices, Union City, CA). Currents were sampled at the rate of 1 kHz, filtered at 500 Hz, and simultaneously stored electronically and displayed in real time. Hemin was diluted to the desired final concentration in ND96 and applied to the oocytes through the perfusion system at a rate of 1 ml/min.

Mass spectrometry: *Sample Preparation- (1D separations was carried out by SM group, may need to be modified)* Samples were denatured in 1xfinal NuPAGE™ LDS Sample Buffer (Cat.#NP0007, Invitrogen), and the resultant enriched proteins were separated onto a NuPAGE™ 10% Bis-Tris Protein gel (Cat.# NP0315BOX, Invitrogen) at 200 V constant for 25min. The gel was stained using a Colloidal Blue Staining Kit (Cat.#LC6025, Invitrogen) following manufacturer's instruction. Each gel lane was excised (two equal-sized fractions pertaining to spectrin alpha and beta molecular weights) and digested overnight at 37 °C with Pierce™ Trypsin Protease, MS Grade (Cat.#90058, Thermo Scientific) as per manufacturer's instruction. Digests were reconstituted in 0.1%FA in 5:95 ACN:ddH2O at ~0.1 μg/uL.

nLC-ESI-MS2 Analysis & Database Searches- Peptide digests (8 μL each) were injected onto a 1260 Infinity nHPLC stack (Agilent Technologies), and separated using a 100 μm I.D. x 13.5 cm pulled tip C-18 column (Jupiter C-18 300 Å, 5 μm, Phenomenex). This system runs in-line with a Thermo Orbitrap Velos Pro hybrid mass spectrometer, equipped with a nano-electrospray source (Thermo Fisher Scientific), and all data were collected in CID mode. The nHPLC was configured with binary mobile phases that included solvent A (0.1%FA in ddH2O), and solvent B (0.1%FA in 15% ddH2O/85% ACN), programmed as follows; 10min @ 5%B (2μL/min, load), 60min @ 5%-40% B (linear: 0.5nL/min, analyze), 5min @ 70%B (2μL/min, wash), 10min @ 0%B (2μL/min, equilibrate). Following each parent ion scan (300–1200 m/z @ 60k resolution), fragmentation data (MS2) was collected on the top most intense 15 ions. For data dependent scans, charge state screening and dynamic exclusion were enabled with a repeat count of 2, repeat duration of 30s, and exclusion duration of 90s.

The XCalibur RAW files were collected in profile mode, centroided and converted to MzXML using ReAdW v. 3.5.1. The data was searched using SEQUEST Version 27, rev. 12 (Thermo Fisher Scientific), which was set for two maximum missed cleavages, a precursor mass window of 20 ppm, trypsin digestion, variable modification P @ −27.9949, R @ −43.0534, K @ −1.0316, T @ −2.0157, C @ 57.0293, and M @ 15.9949. Searches were performed with a mouse-specific subset of the UniRefKB database.

Peptide Filtering, Grouping, and Quantification- The list of peptide IDs generated based on SEQUEST search results were filtered using Scaffold Version 4.8.9 (Protein Sciences, Portland Oregon). Scaffold filters and groups all peptides to generate and retain only high confidence IDs while also generating normalized spectral counts (N-SC's) across all samples for the purpose of relative quantification. The filter cut-off values were set with minimum peptide length of > 5 AA's, with no MH +1 charge states, with peptide probabilities of > 80% C.I., and with the number of peptides per protein ≥2. The protein probabilities were then set to a > 99.0% C.I., and an FDR < 1.0. Scaffold incorporates the two most common methods for statistical validation of large proteome datasets, the false discovery rate (FDR) and protein probability [36–38]. In addition, for all PTM's, we further analyzed the exported Scaffold files within Scaffold PTM (Protein Sciences) where the use of assigned A-scores and localization C.I.'s allowed us to filter out potential false positive PTM assignments [39]. Those PTM's that pass these filters were also manually checked for quality of fit.

Molecular modeling and heme docking: To determine potential mechanisms by which heme exposure impairs ENaC activity within few seconds, we performed computer modeling using YASARA software [40,41] to simulate heme docking and binding to the known cryo-electron microscopy structure of ENaC (Protein Data Bank: 6BQN) [42]. The docking of heme molecule to the ENaC structure was performed using AutoDock program developed at the Scripps Research Institute

using the default docking parameters and point charges initially assigned according to the AMBER03 force field [43], and then damped to mimic the less polar Gasteiger charges used to optimize the AutoDock scoring function. The YASARA molecular modeling program was set up to determine the best 25 hits and also determine their free energy of binding in kJ/mol.

3. Results

Cell-free heme (CFH) and chlorinated lipids are elevated in plasma of humans and animals exposed to Cl_2 gas: Numerous studies including ours have previously shown that plasma levels of CFH are elevated in insults such as toxic halogen gas inhalation, sepsis, hyperoxia, and trauma, which ultimately leads to lung injury [2–10]. However, the mechanisms of increased RBC fragility and plasma CFH are not known. We measured plasma CFH in 5 adult humans, which were admitted to the University of Alabama at Birmingham Emergency Department, post accidental exposure to Cl_2 gas at the Birmingham water treatment plant. The average age of exposed humans was 48 years with 80% of them being males. Blood was also collected from corresponding age and sex matched non exposed humans. Plasma CFH levels were significantly increased in Cl_2 gas exposed patients compared to their sex- and age-matched non-exposed individuals (Fig. 1A). Person exposed to Cl_2 gas also had elevated plasma levels of 16-carbon chlorinated fatty acid (ClFA) (Fig. 1B) and 18-carbon ClFA (Fig. 1C), as measured in plasma obtained from these individuals 3–6 h post exposure in the emergency room. These values were about 20 fold higher

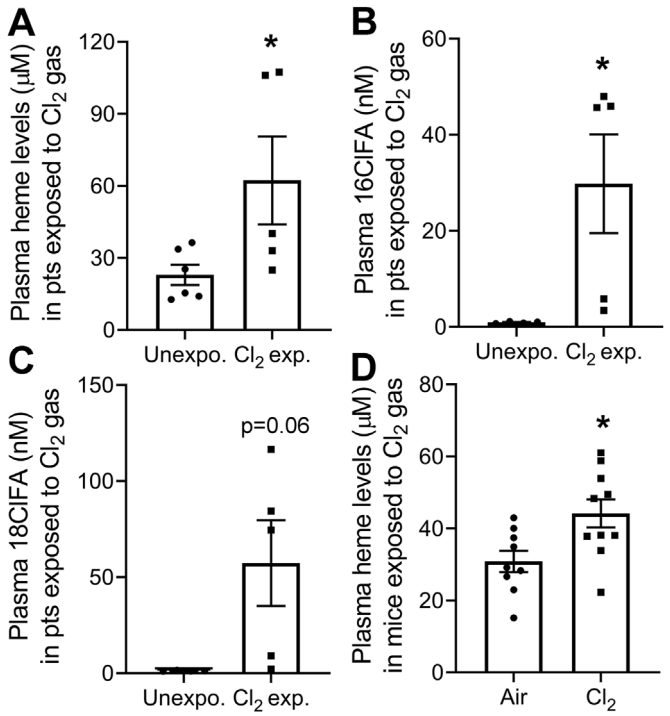

Fig. 1. Plasma cell-free heme (CFH) and chlorinated lipids are elevated in humans and mice exposed to Cl_2 gas. Blood was collected from patients exposed to Cl_2 gas in the emergency room of the University of Alabama at Birmingham, 3–4 h post exposure, stored for 72 h at 4 °C at which time it was analyzed. Blood from human volunteers as controls was treated in the same fashion. Plasma CFH levels in persons exposed to Cl_2 were higher than the age- and sex-matched human controls (n = 5–6) (A). Cl_2 exposed individuals also had elevated levels of 16ClFA (n = 4–5) (B) and 18ClFA (n = 4–5) (C). Similarly, adult male C57BL/6 mice exposed to Cl_2 gas (400 ppm, 30min) had increased levels of heme in plasma 24 h post exposure (n = 9–10) (D). Individual values and means ± SEM. *$P < 0.05$ vs. unexposed humans or air exposed mice; by unpaired *t*-test.

than those found in patients with sepsis [28]. Similarly, exposure of adult C57BL/6 male mice to Cl_2 gas (400 ppm, 30 min) increased plasma levels of CFH levels (24 h post exposure) (Fig. 1D). In addition, we have previously shown that mice exposed to Cl_2 gas also have elevated levels of chlorinated lipids [26].

Halogenated lipids increase RBC hemolysis and cell-free heme: To explore the role of halogenated lipids in increasing RBC fragility and plasma CFH levels, we first determined whether exposure to other halogen gases, such as bromine (Br_2), also increases halogenated lipids. Male C57BL/6 mice were exposed to Br_2 gas (600 ppm, 30min) and then returned to room air. Using LC/MS quantitation, we found that the plasma levels of 16-carbon (Fig. 2A-C) and 18-carbon (Fig. 2D-F) free- and esterified-brominated fatty acids (BrFA) were elevated in the exposed animals. Even at 24 h post exposure, the values of these variables were higher than those measured in patients with ARDS [28]. We also identified elevated levels of brominated fatty aldehyde (BrFALD) in the broncholaveolar lavage fluid (BALF) (Supplementary Figs. 1A and E) of exposed animals. Aldehydes can be oxidized to fatty acids which may exist either in the esterified (bound) or free form [26]. The BALF levels of esterified- and free- BrFA were increased in mice exposed to Br_2 (Supplementary Fig. 1B-D, F-H). The aldehydes can also react with the antioxidant, glutathione, which exists in mM concentrations in the lung epithelial lining and plasma, to form glutathionylated fatty aldehyde (FALD-GSH) [26,31,44]. We found high levels of 16- and 18- carbon FALD-GSH in the BALF (Supplementary Figs. 2A–B), lung (Supplementary Figs. 2C–D), plasma (Supplementary Figs. 3A–B), urine (Supplementary Figs. 3C–D), and RBCs (Supplementary Figs. 3E–F), of Br_2 exposed mice. Because of their high reactivity, aldehydes could not be detected in the plasma in their natural configuration.

Next, to determine if halogenated lipids in the circulation or BALF are responsible for hemolysis and elevated CFH in plasma, RBCs were isolated from air exposed adult male C57BL/6 mice. The RBCs were then incubated *ex vivo* with the 16- and 18- carbon brominated or chlorinated lipids [fatty acid (FA) and fatty aldehyde (FALD), 1 μM each], or their corresponding vehicle (FA and FALD) for 4 h. The RBCs were then subjected to mechanical stress by mixing them with glass beads; the mixtures were shaken for 2 h. Data showed that both the brominated and the chlorinated lipids increased the hemolysis of RBCs significantly (Fig. 3A). In addition, the treatment of RBCs *ex vivo* with either brominated or chlorinated lipids resulted in increased oxidation of RBC membrane proteins, as indicated by elevated levels of carbonyl (aldehydes and ketones) adducts in protein side chains (Fig. 3B and C).

To confirm the presence of carbonylation sites, as an indicator of oxidative stress and damage to RBC, we exposed adult male C57BL/6 mice to either Br_2 (600 ppm, 30min) or Cl_2 (400 ppm, 30min) gas. Twenty four hours post exposure, blood was drawn from these mice and RBC ghosts were isolated. High resolution LCMS2 identified carbonylation changes for 6 putative amino acid sites within the RBC structural protein, spectrin alpha chain, and one site within spectrin beta chain, 24 h post-halogen exposure (Table 1). The sites listed were all confirmed using a number of high confidence filters that included A-score and localization probabilities as indicated in the table and in more detail within the methods section. While exposure to both Br_2 and Cl_2 induced carbonylation, Br_2 appeared to have yielded a higher number of modifications indicating that it may be more damaging. Furthermore, each modification site appeared to be specific to the type of halogen gas, since no overlaps were found between the two exposures. The peptide marked with an asterisk in Table 1 was found to be modified at K1988, and was chosen to be highlighted for the LCMS2 results (Fig. 4), where an example of MS2 spectra are also illustrated to point out how these modifications can be putatively identified. Together, the results indicate that carbonylation of RBC structural proteins may induce hemolysis and increase CFH post exposure to toxic insult.

Heme impairs ENaC activity and Na^+ transport across lung epithelium: We have previously shown that CFH is responsible for lung edema and lung injury post toxic gas inhalation [8–10]. Therefore, to

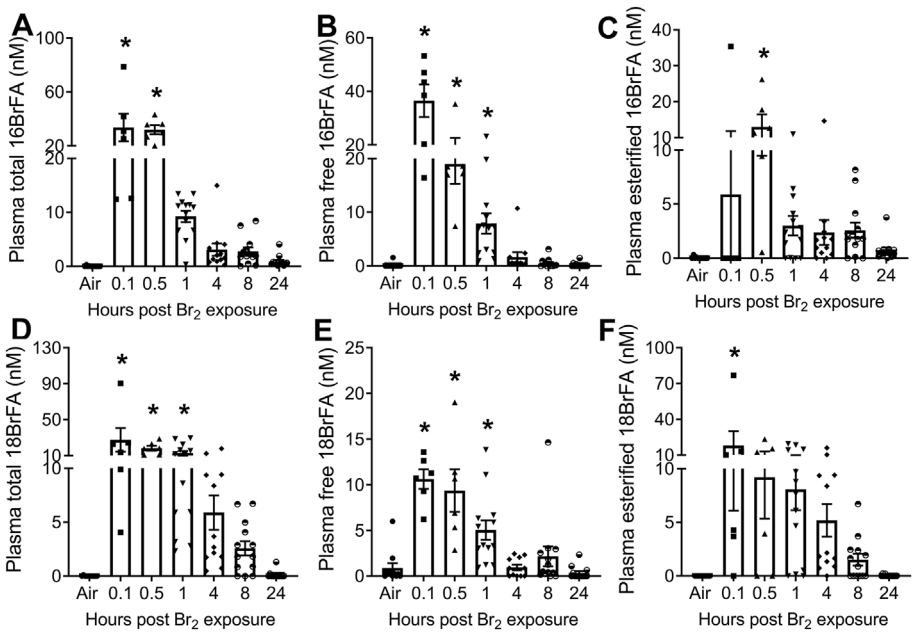

Fig. 2. Brominated fatty acids (BrFA) are elevated in plasma of Br_2 exposed mice. Adult male C57BL/6 mice were exposed to Br_2 gas (600 ppm, 30min) and returned to room air. Using ESI-LC/MS/MS quantitation, total, free, and esterified levels of 16- and 18- carbon BrFA were measured in plasma of mice at different intervals post exposure. The levels of total 16BrFA (n = 6–13) (A), free 16BrFA (n = 6–13) (B), and esterified 16BrFA (C) increased in plasma of Br_2 exposed mice. Similarly, the levels of total 18BrFA (n = 6–13) (D), free 18BrFA (n = 6–13) (E), and esterified 18BrFA (F) increased in plasma of Br_2 exposed mice. Individual values and means ± SEM. *P < 0.05 vs. air exposed mice, by one-way ANOVA followed by Tukey post hoc testing.

determine the mechanism of CFH-induced lung edema, in the first series of experiments, we determined whether heme inhibits active Na^+ transport across human bronchial epithelial cells (HBEC). Although, HBEC are not the primary cells, which are involved in the development of edema, they are Na^+ absorptive, and amiloride-sensitive ENaC-mediated ion transport has been detected in them [45] and are therefore an excellent substitute to study ENaC activity in human cells. Hemin (ferric chloride heme, mentioned just as heme throughout the text) was added in both the apical and basolateral compartments of Ussing chambers mounted with confluent monolayers as previously described [46,47]. Data demonstrated that heme inhibited amiloride-sensitive, ENaC, but not forskolin-stimulated, GlyH-101–inhibited, CFTR, currents within few seconds post exposure (Fig. 5A and B) with an IC_{50} of about 500 nM (Fig. 5C). Transepithelial resistance did not decrease with increased heme concentrations but even at a heme concentration of 10 μM, remained above 1500 Ohms*cm^2, indicating that the monolayers remained intact (data not shown).

In the next series of experiments, we permeabilized the apical membranes of these monolayers and measured the ouabain-sensitive components of Na^+/K^+-ATPase activity. Data showed that heme did not impair (alter) Na^+/K^+-ATPase function even at concentrations that totally inhibited ENaC activity (5–25 μM) (Fig. 5D). To further demonstrate that heme inhibited ENaC, we injected *Xenopus* oocytes with α-, β-, and γ-human ENaC cRNAs and measured current-voltage relationships 48 h later. Oocytes injected with ENaC express significant amounts of Na^+ currents, 90% of which are inhibited by 10 μM amiloride [34]. Treatment of oocytes with 1 μM of heme immediately inhibited whole-cell Na^+ current by 80% (Fig. 6A-C). This decline in whole-cell Na^+ current was similar to amiloride-mediated inhibition of Na^+ current (Fig. 6D-F).

Further, ENaC activity was measured in alveolar type II (AT2) cells in-situ (lung slices) using the cell-attached mode of patch-clamp technique as previously reported [34,48]. Heme was added in the upper portion of the pipette which allowed for the recording of baseline ENaC activity prior to heme reaching the membrane patch under the pipette. Recordings from AT2 cells show the activity of two characteristic conductances: a 4 pS (pS) conductance of the highly Na^+ selective channel (Fig. 7A) and a 16 pS conductance of the non-selective cation channel (Fig. 7E). However, once heme diffused through the pipette and reached the membrane patch under the pipette tip, it decreased the

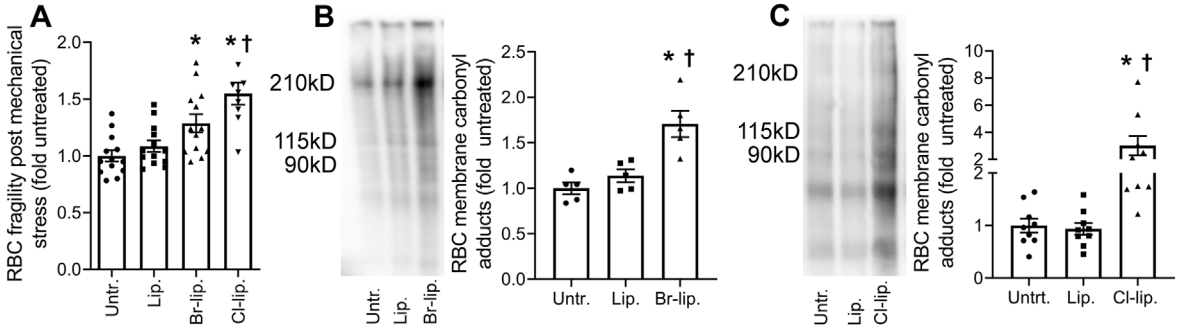

Fig. 3. Halogenated lipids increase carbonylation and hemolysis of RBC. RBCs were isolated from adult male C57BL/6 mice and incubated *ex vivo* with Br-lip (16BrFA, 16BrFALD, 18BrFA, and 18BrFALD, 1 μM each) (n = 13), Cl-lip (16ClFA, 16ClFALD, 18ClFA, 18ClFALD, 1 μM each) (n = 9) in encapsulated liposomes, or equivalent amount of corresponding vehicle (16FA, 16FALD, 18FA, 18FALD, 1 μM each) in encapsulated liposomes. After 4 h incubation with these lipids, mechanical fragility of the cells was tested by mixing the RBCs with glass beads for 2 h and then measuring the released hemoglobin as a result of hemolysis. Both brominated and chlorinated lipids increased RBC hemolysis (A). In another set of experiments RBCs from adult male C57BL/6 mice were incubated *ex vivo* with the same composition of brominated (n = 5) (B) or chlorinated (n = 9) (C) lipids and carbonyl adducts (aldehydes and ketones), a hallmark of the oxidation status of proteins, were measured by gel electrophoresis and western blotting using proteins obtained from the RBCs ghosts. Both Br-lip and Cl-lip increased RBC carbonylation as indicated by increase in protein carbonyl adducts. Individual values and means ± SEM. *P < 0.05 vs. untreated RBCs, †P < 0.05 versus non-halogenated lipids by one-way ANOVA followed by Tukey post hoc testing.

Table 1
Carbonylation of spectrin alpha and beta chains from RBC plasma membranes isolated from mice 24 h post-halogen exposure. Six putative carbonylation sites were confirmed by high resolution tandem mass spectrometry within spectrin alpha chain, and one site was identified within spectrin beta chain post-bromine exposure. These sites were all confirmed with a number of high confidence filters that included A-score and localization probabilities as indicated within the table, and further explained in detail within the methods section. The representative chromatography along with the MS1 & MS2 spectra are further highlighted in Fig. 4.

Spectrin Alpha Chain, Erythocytic Protein (P08032):							
Peptide Carbonylation Modification Site/Sequence	Tx	Localization Probability	A-score	Peptide Probability	Xcorr	*m/z*	Δppm
(K640) QQDFEEELAVNEIMLNNLE***K***	Cl_2	100%	1000	97%	4.1	3	−3.5
(K1401) G***K***CDQVESWMVAR	Br_2	100%	1000	99%	2.7	3	−0.6
(K1484) AL***K***EQLLTELGK	Br_2	100%	152	97%	2.7	2	−0.0
(K1706) MNGVNERFENVQSLAAAHHE***K***	Cl_2	100%	1000	99%	3.7	3	−2.9
(K1988) LSEIAEL***K***DQLVAGEHSQAK*	Br_2	100%	165	100%	5.5	3	−1.7
(K2259) MQHNLEQQIQA***K***DTIGVSEETLKEFSTTYK	Br_2	100%	25	96%	3.3	5	−7.1
Spectrin Beta Chain, Erythocytic Protein (P15508):							
Peptide Modification Site/Sequence	Tx	Localization Probability	A-score	Peptide Probability	Xcorr	*m/z*	Δppm
(K960) *VNNYCVDCEETS**K**WIMDK*	Br_2	100%	88	100%	4.6	2	8.0

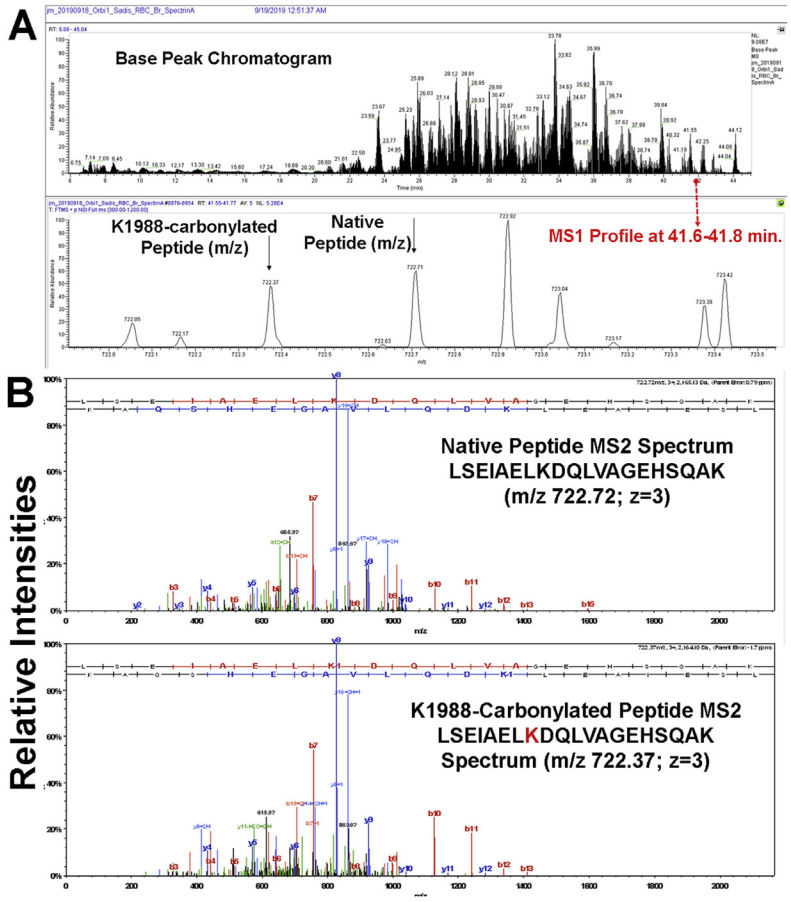

C
Native Peptide MS2 Fragment Table (LSEIAELKDQLVAGEHSQAK)

B	B Ions	B+2H	B-NH3	B-H2O	AA	Y Ions	Y+2H	Y-NH3	Y-H2O	Y
1	114.1	57.5			L	2,166.1	1,083.6	2,149.1	2,148.1	20
2	201.1	101.1		183.1	S	2,053.1	1,027.0	2,036.0	2,035.0	19
3	330.2	165.6		312.2	E	1,966.0	983.5	1,949.0	1,948.0	18
4	443.3	222.1		425.2	I	1,837.0	919.0	1,820.0	1,819.0	17
5	514.3	257.6		496.3	A	1,723.9	862.5	1,706.9	1,705.9	16
6	643.3	322.2		625.3	E	1,652.9	826.9	1,635.8	1,634.8	15
7	756.4	378.7		738.4	L	1,523.8	762.4	1,506.8	1,505.8	14
8	884.5	442.8	867.5	866.5	K	1,410.7	705.9	1,393.7	1,392.7	13
9	999.5	500.3	982.5	981.5	D	1,282.6	641.8	1,265.6	1,264.6	12
10	1,127.6	564.3	1,110.6	1,109.6	Q	1,167.6	584.3	1,150.6	1,149.6	11
11	1,240.7	620.8	1,223.7	1,222.7	L	1,039.6	520.3	1,022.5	1,021.5	10
12	1,339.7	670.4	1,322.7	1,321.7	V	926.5	463.7	909.4	908.5	9
13	1,410.8	705.9	1,393.8	1,392.8	A	827.4	414.2	810.4	809.4	8
14	1,467.8	734.4	1,450.8	1,449.8	G	756.4	378.7	739.3	738.4	7
15	1,596.8	798.9	1,579.8	1,578.8	E	699.3	350.2	682.3	681.3	6
16	1,733.9	867.5	1,716.9	1,715.9	H	570.3	285.7	553.3	552.3	5
17	1,820.9	911.0	1,803.9	1,802.9	S	433.2	217.1	416.2	415.2	4
18	1,949.0	975.0	1,932.0	1,931.0	Q	346.2	173.6	329.2		3
19	2,020.0	1,010.5	2,003.0	2,002.0	A	218.1	109.6	201.1		2
20	2,166.1	1,083.6	2,149.1	2,148.1	K	147.1	74.1	130.1		1

D
K1988-Carbonylated Peptide Fragment Table (LSEIAELKDQLVAGEHSQAK)

B	B Ions	B+2H	B-NH3	B-H2O	AA	Y Ions	Y+2H	Y-NH3	Y-H2O	Y
1	114.1	57.5			L	2,165.1	1,083.1	2,148.1	2,147.1	20
2	201.1	101.1		183.1	S	2,052.0	1,026.5	2,035.0	2,034.0	19
3	330.2	165.6		312.2	E	1,965.0	983.0	1,948.0	1,947.0	18
4	443.3	222.1		425.2	I	1,835.9	918.5	1,818.9	1,817.9	17
5	514.3	257.6		496.3	A	1,722.9	861.9	1,705.8	1,704.9	16
6	643.3	322.2		625.3	E	1,651.8	826.4	1,634.8	1,633.8	15
7	756.4	378.7		738.4	L	1,522.8	761.9	1,505.8	1,504.8	14
8	883.5	442.2	866.5	865.5	K-1	1,409.7	705.4	1,392.7	1,391.7	13
9	998.5	499.8	981.5	980.5	D	1,282.6	641.8	1,265.6	1,264.6	12
10	1,126.6	563.8	1,109.5	1,108.6	Q	1,167.6	584.3	1,150.6	1,149.6	11
11	1,239.6	620.3	1,222.6	1,221.6	L	1,039.6	520.3	1,022.5	1,021.5	10
12	1,338.7	669.9	1,321.7	1,320.7	V	926.5	463.7	909.4	908.5	9
13	1,409.8	705.4	1,392.7	1,391.7	A	827.4	414.2	810.4	809.4	8
14	1,466.8	733.9	1,449.7	1,448.8	G	756.4	378.7	739.3	738.4	7
15	1,595.8	798.4	1,578.8	1,577.8	E	699.3	350.2	682.3	681.3	6
16	1,732.9	866.9	1,715.8	1,714.9	H	570.3	285.7	553.3	552.3	5
17	1,819.9	910.5	1,802.9	1,801.9	S	433.2	217.1	416.2	415.2	4
18	1,948.0	974.5	1,930.9	1,930.0	Q	346.2	173.6	329.2		3
19	2,019.0	1,010.0	2,002.0	2,001.0	A	218.1	109.6	201.1		2
20	2,165.1	1,083.1	2,148.1	2,147.1	K	147.1	74.1	130.1		1

Fig. 4. Halogen gas exposure increased carbonylation of RBC spectrin A and B chains in mice. A representative LCMS2 analysis is illustrated with a focus on the tryptic peptide (LSEIAELKDQLVAGEHSQAK) from spectrin alpha chain as highlighted in Table 1 (A) Illustration of the LCMS base-peak chromatogram, (B) parent-ion spectra from the peptide peaks of interest using data dependent analysis at 41.7 min along with the resulting MS2 spectra for those ions representing the native (top) vs. Ox-K1988 (bottom) peptide of interest. The tables, (C) native peptide, and (D) Ox-K1988 peptide represent the corresponding fragments for the peptides from the MS2 spectra. The highlighted sections (b-ions/orange, y-ions/blue) represent those fragments that were observed in the MS2 spectra. The MS2 spectra illustrate that the two peptides (native vs. modified) fragment are nearly identically at charge state 3, with only 1-Da shifts that indicate K1988 is modified, which is made clear in the fragmentation tables. It's noted that all the 1-Da fragmentation shifts between the two tables are apparent below the b-8 ion and above the y-13 ion, both corresponding with AA#8 (K1988). MS was performed from RBC ghosts pooled from 4 to 5 animals. (For interpretation of the references to colour in this figure legend, the reader is referred to the Web version of this article.)

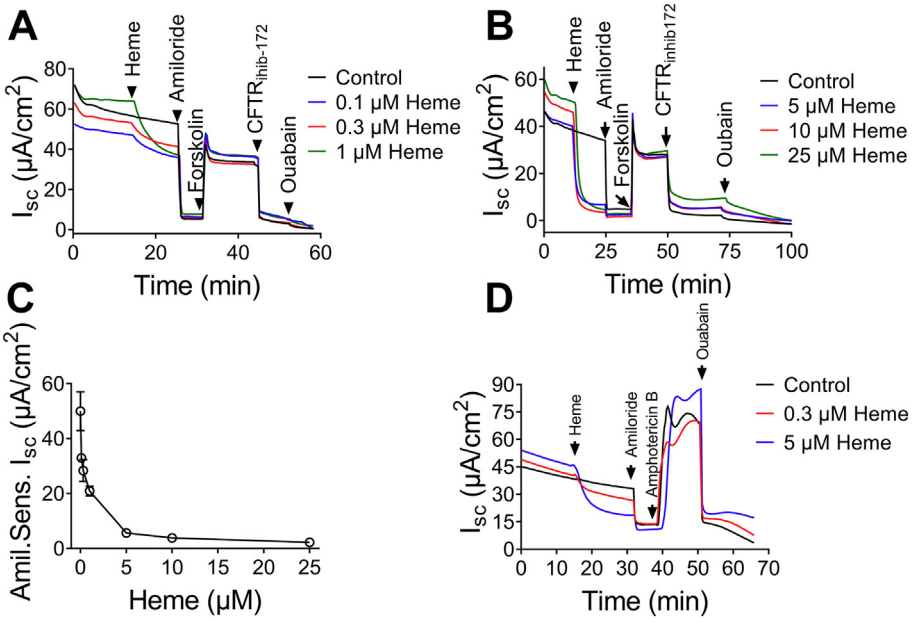

Fig. 5. Heme impairs short circuit current (Isc) in human bronchiolar epithelial cells. Panels (A) and (B) illustrate the dose response of heme on short circuit current recorded from human bronchiolar epithelial cells monolayers mounted in Ussing chambers. Heme significantly reduced amiloride sensitive Na^+ current in a dose-response fashion within seconds from its addition in the apical chamber but had no effect on the forskolin activated chloride current. The rate of Na^+ current inhibition by heme is similar to Na^+ current inhibition by amiloride (n = 7). Panel (C) summarizes the dose response of Na^+ current to increasing heme concentrations (n = 7). Values are means ± 1 SEM. Further, cell monolayers were mounted on the Ussing system, Na^+ current was inhibited by the addition of amiloride (10 μM) or heme (5 μM) in the apical compartment; then the apical membranes were permeabilized by the addition of amphotericin B in the apical compartment and after the current had stabilized, ouabain was added into the basolateral compartment. The difference in current prior to and following ouabain addition represents the Na^+/K^+-ATPase (pump current). The data shows that heme does not inhibit the pump current (n = 7). The graphs are representative of experiment which was repeated 7 times.

open probabilities of both the 4 pS (Fig. 7B and C) and 16 pS channels (Fig. 7F and G) with an IC_{50} of 125 nM for both 4 pS (Figs. 7D) and 16 pS (Fig. 7H).

To further understand the mechanism by which CFH instantaneously inhibits ENaC activity and Na^+ conductance across the lung epithelium, we performed computer modeling using YASARA software [40,41] to identify potential heme binding sites and their potential ability to block Na^+ conductance. For this purpose, we used a recently developed cryo-electron microscopy structure of ENaC (Protein Data Bank: 6BQN) [42]. The ion channel has large extracellular domains and a narrow transmembrane pore and the α:β:γ subunits are arranged in a counter-clockwise manner in a 1:1:1 stoichiometry [42]. The software predicted 22 potential docking sites of heme on ENaC with the energy of binding ranging from 86 to 1563 kJ/mol. Close analysis of these docking sites showed that at least two heme-bonding sites are located within the ENaC transmembrane pore (energy of binding 390.5 and 313.2 kJ/mol) (Fig. 8A and B), which can potentially block Na^+ transport through the channel. Together, these results demonstrated that heme mediated decrease in ENaC activity may be responsible for lung edema during ARDS.

Heme scavenging attenuates RBC hemolysis and improved ENaC activity post halogen gas exposure: Next, we determined whether scavenging CFH would improve the integrity of RBC's plasma membrane and prevent hemolysis. We exposed C57BL/6 mice to Br_2 (600 ppm) or Cl_2 (400 ppm) for 30 min and then treated the mice with an intramuscular injection of the heme scavenging protein, hemopexin, (4 mg/kg BW) 1 h later as published earlier [8,9]. The plasma bioavailability of hemopexin in a 25 g mouse receiving 100 μg hemopexin intramuscularly is about 25 μg/ml (total volume of blood in a 25 g mouse is about 1 ml) for at least 24 h. The serum half-life of hemopexin is approximately 7 days, while that of heme-Hx complex is about 7 h [49]]. The RBCs were isolated from mice 1 day post exposure. Results demonstrated that hemopexin attenuated RBC plasma membrane protein carbonyl adducts post Br_2 (Fig. 9A) and Cl_2 (Fig. 9B) gas exposure. The exposure of isolated RBC to mechanical stress also showed that hemopexin reduced RBC hemolysis in the RBCs obtained from mice exposed to Br_2 or Cl_2 gas (Fig. 9C).

Lastly, we determined whether heme scavenging would improve

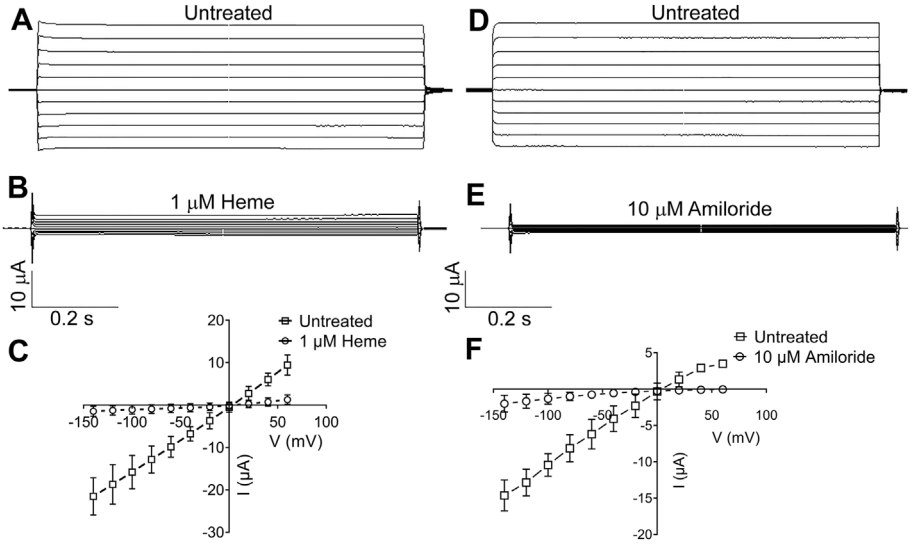

Fig. 6. Heme inhibits ENaC heterologously expressed in oocytes. Panel (A) shows whole cell total current recording using the double voltage clamp technique from an oocyte 24 h post injection of human –αβγ ENaC. Panel (B) shows that Na^+ current is inhibited by 5 μM heme in the bath. Panel (C) shows current-voltage relationships of total currents expressed in ENaC injected oocytes following perfusion with hemin or saline. (n = 11). Panels (D), (E), and (F) show a comparable inhibition of whole cell total current in oocytes by amiloride (n = 11). Values are means ± SEM.

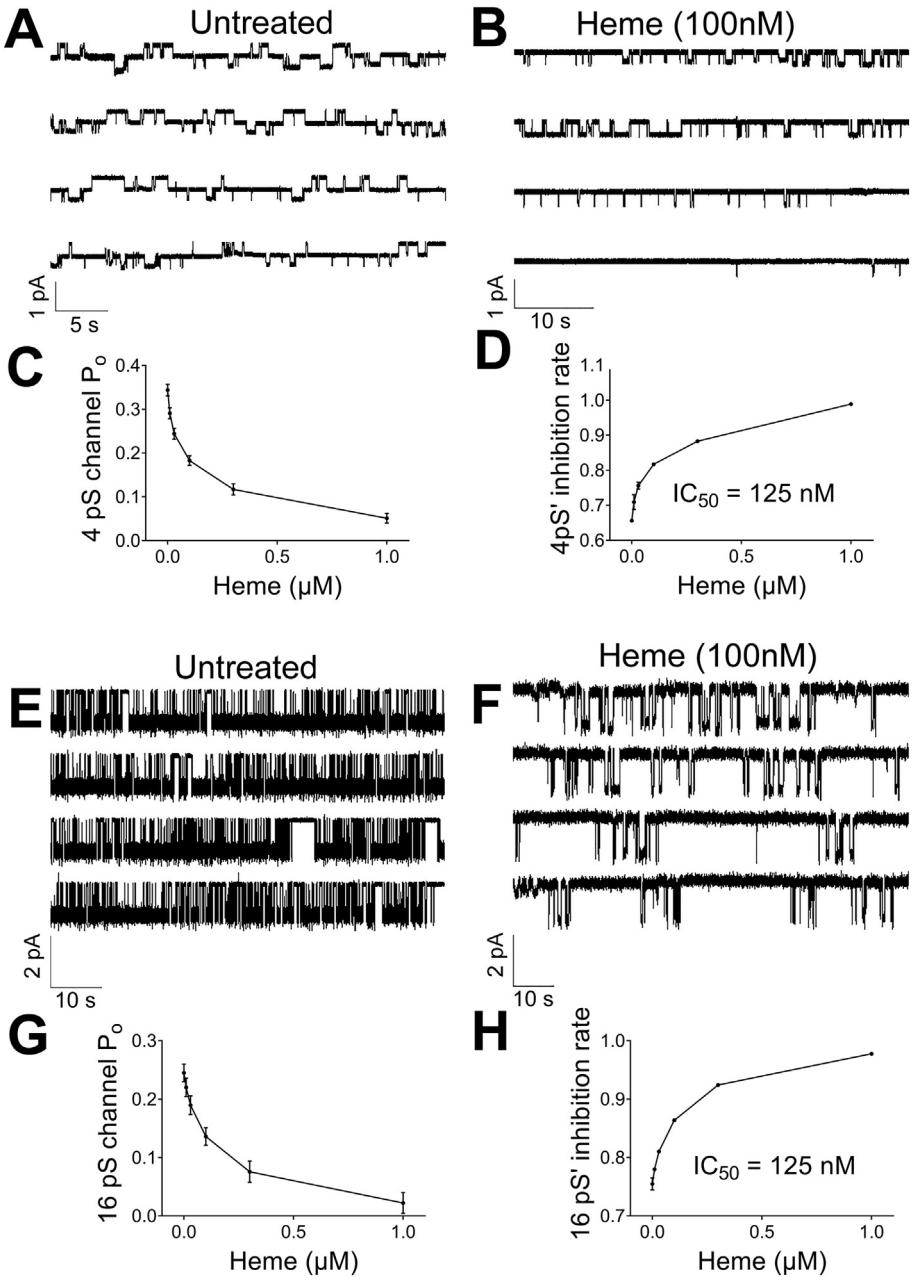

Fig. 7. Heme inhibits ENaC activity in AT2 cells in situ. AT2 cells in lung slices were patched in the cell-attached mode. The top portion of the pipette was filled with heme so the overall concentration of heme in the pipette was 100 nM. Panel (A) represents a typical trace exhibiting mainly the 4 pS amiloride-sensitive current (ENaC). Notice the inhibition of ENaC activity as heme diffuses towards the patch under the pipette (B). Panel (C) shows the inhibition of open probability (P_0) of 4 pS channel at increasing heme concentrations (0.01–1000 nM) in the pipette (n = 9). Panel (D) illustrates the rate of ENaC inhibition by increasing heme concentrations: 10 nM, 30 nM, 100 nM, 300 nM and 1 μM. The IC_{50} was 125 nM (n = 9). Panel (E) shows a record of AT2 channel activity in which the cation (16 pS) was very prominent. As in panel A, the top portion of the pipette was filled with heme so the overall concentration of heme in the pipette was 100 nM. Note the slow decrease of channel's activity with time as heme reaches the membrane patch under the pipette (F). Panel (G) shows the open probability of 16 pS channel at increasing heme concentration in the pipette (same as above). Panel H shows that the IC_{50} was again 125 nM (n = 10). Values are means ± 1 SEM.

ENaC activity by increasing the open probability (P_0) of 4 pS and 16 pS channels in a mouse model of Br_2 induced lung injury. Adult male C57BL/6 mice were exposed to air or Br_2 and tehn treated with either saline or hemopexin (4 mg/kg BW) as mentioned above. Mice were sacrificed 24 h post exposure and lungs were isolated. AT2 cells in lung slices were patched in the cell-attached mode. Our data showed that the open probability of 4 pS (Fig. 10 A–D) and 16 pS (Fig. 10 E–H) was significantly attenuated after Br_2 exposure. However, mice that were treated with hemopexin after Br_2 exposure had significant recovery in the open probability of both the 4 pS (Fig. 10 A–D) and 16 pS (Fig. 10 E–H) channels. Together these results show that CFH released post exposure to halogen gas or halogenated lipids exaggerates RBC hemolysis and further contributes to RBC defect. The scavenging of free heme by hemopexin not only reduces RBC hemolysis, it also improves the activity of ENaC post lung injury.

4. Discussion

ARDS is a common and severely morbid syndrome with high mortality despite years of advances in the understanding and management of this complex illness. Although several scientific theories on the pathogenesis of ARDS have developed in animals, they are often difficult to test in humans due to many clinical variables. We have previously established an animal model of inhalation lung injury and ARDS, where C57BL/6 mice were exposed to halogen gases such as Cl_2, Br_2, or phosgene ($COCl_2$) [8–10,50,51]. One day post exposure, rodents exposed to these agents developed lung pathology similar to ARDS patients such as accumulation of protein rich fluid in alveoli, migration of peripheral immune cells in the lung, and release of cytokines and chemokines in lung and plasma; a significant portion died within the first 48 h post exposure from respiratory failure [9,10]. Those which survived developed peribronchial fibrosis and pulmonary emphysema [8]. Interestingly, we also found that the rodents exposed to toxic gases such as Br_2 or $COCl_2$ had elevated plasma and BALF levels of CFH

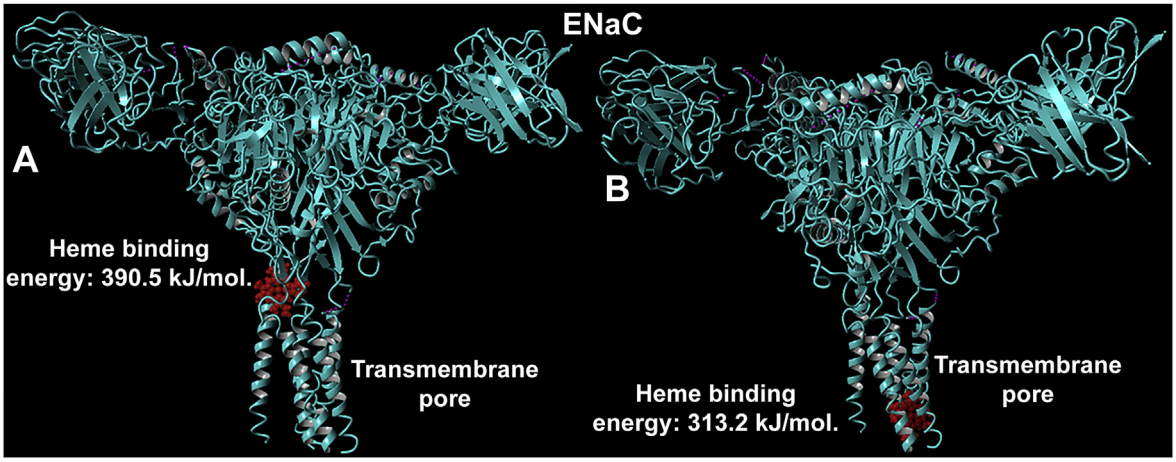

Fig. 8. Computer modeling and heme docking on ENaC. The YASARA computer modeling software was used to identify heme binding sites on the known ENaC structure (Protein Data Bank: 6BQN). The AutoDock program was utilized to dock heme molecules on ENaC. The software identified 22 heme docking sites on ENaC. Two prominent heme (red balls) docking sites within the transmembrane domain are highlighted in the figure. The energy of heme binding to ENaC at these two sites was determined by the software as 390.5 kJ/mol (A) and 313.2 kJ/mol. (For interpretation of the references to colour in this figure legend, the reader is referred to the Web version of this article.)

[8–10]. The administration of the heme scavenging protein, hemopexin, or the overexpression of the heme degrading enzyme, heme-oxygenase 1 (HO-1), in Br_2 exposed animals resulted in significant reduction of lung edema and inflammation [8,9].

Hemolysis has been reported in several clinical conditions [2–10]. Under hemolytic states, the physiological mechanisms for removing CFH from the circulation or heme detoxification systems get overwhelmed, which allows for nonspecific heme uptake and heme catalyzed oxidation reactions [52–54]. In this manuscript we report for the first time, an increase in the plasma levels of CFH in humans who were exposed to Cl_2 gas post accidental gas leakage at the Birmingham Water Works Plant on February 27th, 2019. These findings correlated with our rodent experiments, where we found that C57BL/6 mice exposed to Cl_2 gas also had elevated plasma levels of CFH. Since halogen gases such as Cl_2 and Br_2 do not cross alveolar epithelium post inhalation, to reach blood stream, they are unlikely to cause hemolysis. However, we had earlier reported that rodents exposed to Cl_2 gas had elevated plasma levels of chlorinated fatty acids (ClFA), which are formed by the interaction of Cl_2 with plasmalogens on the alveolar epithelium [26]. Therefore, we sought to determine whether these longer lasting, modified lipids, are the catalyst for hemolysis and elevated CFH in animals and humans. *Ex vivo* exposure of RBCs to chlorinated or brominated lipids in concentrations similar to seen in animals post halogen gas exposure resulted in hemolysis and release of CFH. Interestingly, we found that ClFA were also elevated in humans that were accidently exposed to Cl_2 gas suggesting that halogenated lipids may be responsible for hemolysis post inhalation of toxic gases. Moreover, recent studies have shown that these halogenated lipids are elevated in patients who have ARDS secondary to sepsis and correlate with the disease severity [28]. In these patients, chlorinated and brominated lipids are increased as an end product of reactions by myeloperoxidase (MPO) and eosinophil peroxidase (EPO) respectively [55]. Thus, our data establishes that halogenated lipids are both biomarkers and potential mediators of hemolysis and acute lung injury.

Additionally, an increase in plasma CFH can itself cause substantial hemolysis by stimulating potassium loss and impairing the ability of RBCs to maintain cation gradient [56]. CFH also disrupt lipid–lipid, lipid–protein, and protein–protein associations in RBC ghosts [57]. Earlier studies have shown CFH can destabilize RBC membrane by altering the conformation of cytoskeletal proteins, such as spectrin and protein 4.1 [58]. The hydrophobic molecule, CFH, enters RBC membrane and interacts with hydrogen peroxide to cause oxidative modification of cytoskeletal proteins [59]. Oxidation of amino acid residues in spectrin can result in the aggregation of the protein, which may cause

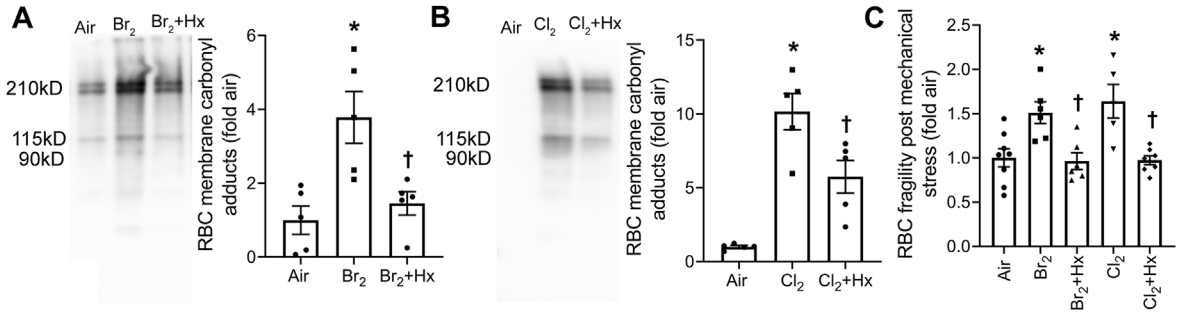

Fig. 9. Heme scavenging attenuates RBC membrane protein oxidation and RBC fragility. Adult male C57BL/6 mice were exposed to Br_2 (600 ppm, 30min) or Cl_2 (400 ppm, 30min) gas and returned them to room air. One hour later, mice were given an intramuscular injection of either saline or hemopexin (Hx) (4 mg/kg BW). Mice were sacrificed 24 h post exposure and the RBCs were isolated. The carbonyl (aldehydes and ketones) adducts, a hallmark of the oxidation status of proteins, were measured by gel electrophoresis and western blotting using proteins obtained from the RBCs ghosts. The data demonstrated that Hx attenuated Br_2 (n = 5) (A) and Cl_2 (n = 5–6) (B) induced increase in RBC membrane protein oxidation. Further, subjecting the isolated RBCs to mechanical stress, showed that Hx treatment prevented the increase in RBC fragility and hemolysis induced by exposure of mice to the halogen gases (n = 5–8) (C). Individual values and means ± SEM. $^{*}P < 0.05$ vs. air exposed mice, $^{\dagger}P < 0.05$ vs. mice exposed to Br_2 for panel A, Cl_2 for panel B, and their respective Br_2 or Cl_2 for panel C. The results were analyzed by one-way ANOVA followed by Tukey post hoc testing.

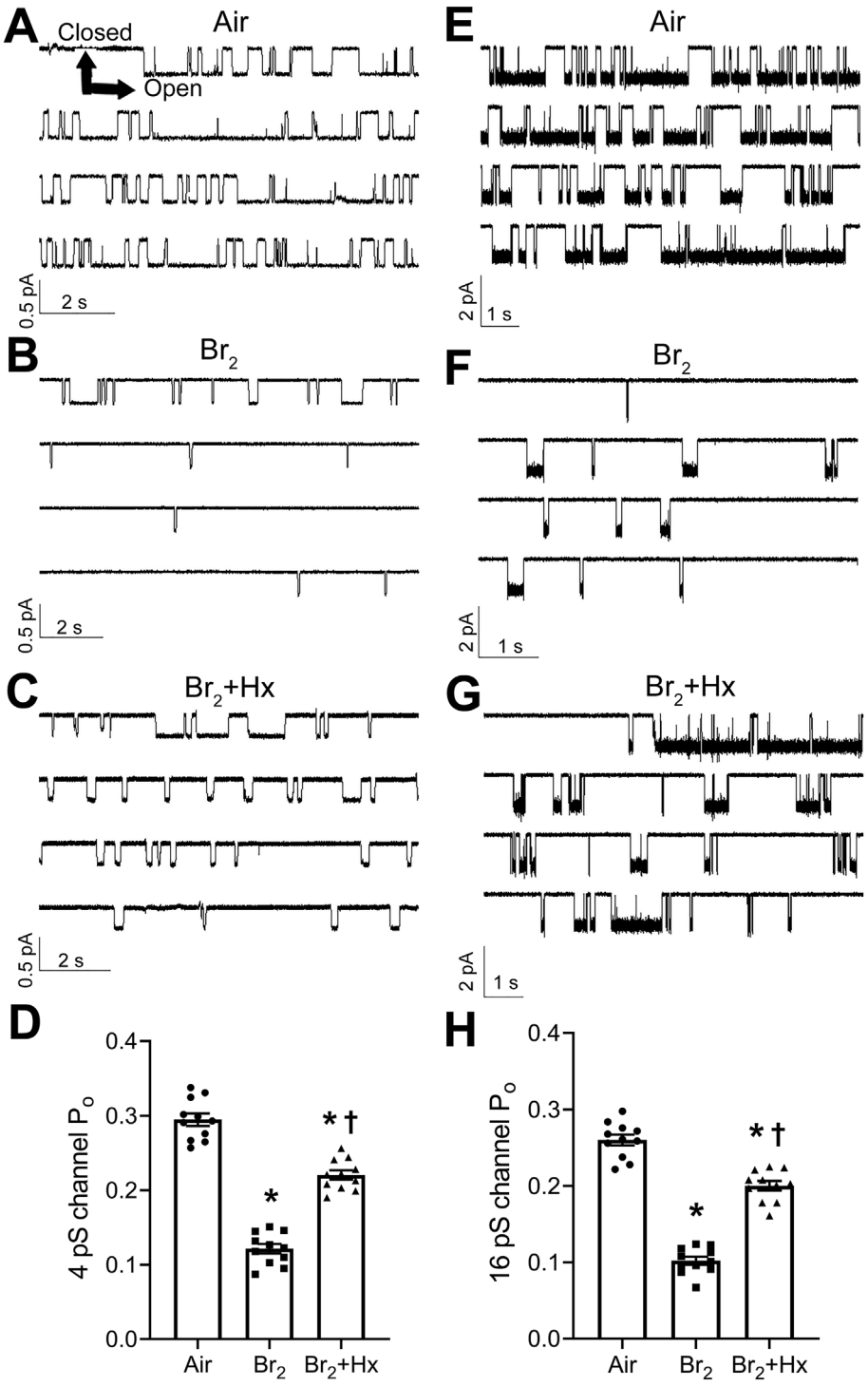

Fig. 10. Heme scavenging improves EnaC function. Adult male C57BL/6 mice were exposed to air or Br_2 (600 ppm, 30min) gas and returned them to room air. One hour later, mice were given an intramuscular injection of either saline or hemopexin (Hx) (4 mg/kg BW). Mice were sacrificed 24 h post exposure and lungs were isolated. AT2 cells in lung slices were patched in the cell-attached mode. Panel (A–C) represents trace exhibiting mainly the 4 pS, while panel (E–G) represents trace exhibiting mainly the 16 pS, amiloride-sensitive current (ENaC) in the air, Br_2, or Br_2 + Hx treated mice. Notice the inhibition of open probability (P_0) of 4 pS and 16 pS channels in the Br_2 exposed mice AT2 cells (B, F). However, the P_0 of 4 pS and 16 pS channels was significantly improved in the AT2 cells of mice treated with Hx post Br_2 exposure. Panel (D–H) shows the quantification of P_0 of 4 pS and 16 pS channels respectively. Individual values and means ± SEM. (n = 11). $^*P < 0.05$ vs. air exposed mice, $^{\dagger}P < 0.05$ vs. mice exposed to Br_2 for panels D and H. The results were analyzed by one-way ANOVA followed by Tukey post hoc testing.

a decrease in spectrin content on the RBC membrane [60]. In the present study, we found that the exposure to Cl_2 or Br_2 gas resulted in the post translational modification (carbonylation, a read out of oxidative stress) of the lysine residues in spectrin alpha and beta chains. Interestingly, we report for the first time that Cl_2 and Br_2 gases caused carbonylation of distinct lysine residues in spectrin. Specifically, Br_2 was able to cause carbonylation of both alpha and beta chains of spectrin, while Cl_2 exposure caused the carbonylation in spectrin alpha chain only. These results suggest that the initial hemolysis and release of CFH by halogenated lipids can potentially be self-propagated by CFH in ARDS resulting in continued hemolysis even when the initial insult ceases to exist.

Recent studies have shown that CFH disrupts alveolar-capillary barrier [20]. A functional alveolar epithelial barrier is vital for optimal fluid balance and gas exchange in the lung [61,62]. Excess alveolar fluid from the air space is reabsorbed into the interstitium by active Na^+ transport process in which Na^+ enters the alveolar epithelial cells through the apically located ENaC and cation channels and is pumped out subsequently by the basolaterally located Na^+/K^+-ATPase [61,63]. Mice lacking ENaC are unable to clear lung fluid from the alveoli and die immediately after birth [64]. Importantly, in most ARDS patients, alveolar fluid clearance (AFC) is impaired [22]. Moreover, the mortality is significant higher in ARDS patients with impaired AFC than in ARDS patients with normal AFC [22] suggesting that ENaC dysfunction is

critical in ARDS pathology. In addition, increased concentration of reactive intermediates following various forms of lung injury have been shown to also inhibit the Na^+/K^+-ATPase which abolishes active Na^+ transport leading to alveolar edema [65–69]. However, data presented herein clearly establish that in our models of lung injury, Na^+/K^+-ATPase is not inhibited and the decrease in short circuit current across cultured human airway cells post heme exposure is due to damage to the apically located Na^+ conducting pathways, including ENaC.

ENaC is composed of 3 homologous subunits α, β and γ [70,71]. At the single channel level, ENaC is highly selective for Na^+ over K^+ with low conductance (~4 pS) with prolonged channel opening. ENaC activity is blocked by the potassium-sparing diuretic, amiloride, with a K_i of around 100 nM [72]. ENaC activity can be altered significantly in two ways. Firstly, a rapid alteration in Na^+ conduction through ENaC can be achieved by changing the open probability (P_o) or open state of the channel [73]. The decline in open probability results in decreased Na^+ transport without a change in the surface expression of the channel. Secondly, Na^+ reabsorption through ENaC can be changed by altering the number of channels located in the apical membrane [74–76]. In the present study, we found that heme rapidly (within few seconds) reduced the open probability of the 4 and 16 pS channels with an IC_{50} of 125 nM in mouse lung slices. However, the activity of the Na^+/K^+-ATPase or the cyclic AMP (cAMP)-activated chloride (Cl^-) channel, CFTR, was not altered by heme exposure. In a different study, heme has been shown to reduce the open probability of ENaC in mouse kidney cortical-collecting duct cells with an IC_{50} of 23.3 nM [77]. The difference in the IC_{50} seen in our study could be explained by the different techniques used in each study. We applied heme to the outer side of the membrane, cell attached mode, while Wang et al. applied heme to the inner side of the membrane using the inside-out configuration of the patch clamp [77]. It is likely that the site to which heme binds ENaC and blocks the channel is closer to the inner narrower side of the transmembrane pore as shown in our model of putative heme binding sites on ENaC. In addition, the response of heme to particular cell and tissue type may be different since we used lung tissues and the other study used cultured kidney cells [77].

There are no known heme binding sites on ENaC. Therefore, to identify these potential sites of ENaC, we performed computer modeling using a known cryo-electron microscopy structure of ENaC [42]. The software predicted 22 potential docking sites of heme molecule on ENaC with the energy of binding ranging from 86 to 1563 kJ/mol. In particular, we found that at least two these heme-bonding sites were located near both ends of the narrow transmembrane pore of ENaC (energy of binding 390.5 and 313.2 kJ/mol). Therefore, it is entirely possible that the relative large molecular mass of the heme molecule (616.5 Da) blocks the pore of the channel and prevents the transportation of a smaller ion such as Na^+ (22.9 Da). This would explain the immediate response of heme to Na^+ transport. Previous studies on BK (calcium-activated potassium) channels have demonstrated that the CXXCH amino acid sequence serves as a conserved heme-binding motif [78]. However, no individual ENaC subunit contains this motif and therefore it is possible that the combined allosteric structure of the 3 ENaC subunits provide basis for heme interaction. Further investigation involving truncation, replacement, or mutation of regions within the subunits will be required to fully understand this phenomenon. Since in our study, heme did not alter the activity of the Na^+/K^+-ATPase or the cyclic AMP (cAMP)-activated chloride (Cl^-) channel, it also signifies that the inhibition by heme is channel specific.

To determine the role of heme scavenging strategy as a potential therapeutic approach to mitigate the impairment of ENaC activity, we exposed C57BL/6 mice to Br_2 gas and then treated them with an intramuscular injection of the purified heme scavenging protein, hemeopexin. The data showed that exposure to Br_2 significantly reduced the open probability of the 4 pS and the 16 pS ENaC channels. We have similarly previously shown that the exposure to Cl_2 gas also impairs ENaC channel activity and alveolar fluid clearance, leading to pulmonary edema [79]. Interestingly, in the current study we found that treatment of Br2 exposed mice with hemopexin reversed the effects of Br_2 and increased the open probability of the 4 pS and 16 pS channels. This data suggest that heme may be an important driver of impaired fluid clearance and lung edema in ARDS and strategies aimed at reducing the levels of free heme in ARDS may play an important role as adjuvant therapy to reduce morbidity and mortality.

Declaration of competing interest

The authors have declared that no conflict of interest exists.

Acknowledgements

The authors would like to thank Dr. Rakesh Patel, Dr. Tamas Jilling for their valuable inputs. In addition, the authors would like to acknowledge technical support of Mark A. Duerr, Jacob D. Franke, and Carolyn J. Albert in the generation of the brominated lipid data.

Appendix A. Supplementary data

Supplementary data to this article can be found online at https://doi.org/10.1016/j.redox.2020.101592.

Funding

This work was supported by the CounterACT Program, National Institutes of Health Office of the Director (NIH OD), the National Institute of Neurological Disorders and Stroke (NINDS), and the National Institute of Environmental Health Sciences (NIEHS), Grant Numbers (5UO1 ES026458; 3UO1 ES026458 03S1; 5UO1 ES027697) to **SM** and NIH/NHLBI grant K12 HL143958 to **SA**.

References

[1] S.W. Ryter, R.M. Tyrrell, The heme synthesis and degradation pathways: role in oxidant sensitivity. Heme oxygenase has both pro- and antioxidant properties, Free Radic. Biol. Med. 28 (2000) 289–309.
[2] L. Li, B. Frei, Prolonged exposure to LPS increases iron, heme, and p22phox levels and NADPH oxidase activity in human aortic endothelial cells: inhibition by desferrioxamine, Arterioscler. Thromb. Vasc. Biol. 29 (2009) 732–738.
[3] J.H. Shannahan, A.J. Ghio, M.C. Schladweiler, J.K. McGee, J.H. Richards, S.H. Gavett, U.P. Kodavanti, The role of iron in Libby amphibole-induced acute lung injury and inflammation, Inhal. Toxicol. 23 (2011) 313–323.
[4] P.A. Dennery, G. Visner, Y. Weng, X. Nguyen, F. Lu, D. Zander, G. Yang, Resistance to hyperoxia with heme oxygenase-1 disruption: role of iron, Free Radical Biol. Med. 34 (2003) 124–133.
[5] G.J. Kato, M.H. Steinberg, M.T. Gladwin, Intravascular hemolysis and the pathophysiology of sickle cell disease, J. Clin. Investig. 127 (2017) 750–760.
[6] R. Stapley, C. Rodriguez, J.Y. Oh, J. Honavar, A. Brandon, B.M. Wagener, M.B. Marques, J.A. Weinberg, J.D. Kerby, J.F. Pittet, R.P. Patel, Red blood cell washing, nitrite therapy, and antiheme therapies prevent stored red blood cell toxicity after trauma-hemorrhage, Free Radic. Biol. Med. 85 (2015) 207–218.
[7] T. Lin, D. Maita, S.R. Thundivalappil, F.E. Riley, J. Hambsch, L.J. Van Marter, H.A. Christou, L. Berra, S. Fagan, D.C. Christiani, H.S. Warren, Hemopexin in severe inflammation and infection: mouse models and human diseases, Crit. Care 19 (2015) 166.
[8] S. Aggarwal, I. Ahmad, A. Lam, M.A. Carlisle, C. Li, J.M. Wells, S.V. Raju, M. Athar, S.M. Rowe, M.T. Dransfield, S. Matalon, Heme scavenging reduces pulmonary endoplasmic reticulum stress, fibrosis, and emphysema, JCI Insight 3 (2018).
[9] S. Aggarwal, A. Lam, S. Bolisetty, M.A. Carlisle, A. Traylor, A. Agarwal, S. Matalon, Heme attenuation ameliorates irritant gas inhalation-induced acute lung injury, Antioxidants Redox Signal. 24 (2016) 99–112.
[10] S. Aggarwal, T. Jilling, S. Doran, I. Ahmad, J.E. Eagen, S. Gu, M. Gillespie, C.J. Albert, D. Ford, J.Y. Oh, R.P. Patel, S. Matalon, Phosgene inhalation causes hemolysis and acute lung injury, Toxicol. Lett. 312 (2019) 204–213.
[11] A.N. Higdon, G.A. Benavides, B.K. Chacko, X. Ouyang, M.S. Johnson, A. Landar, J. Zhang, V.M. Darley-Usmar, Hemin causes mitochondrial dysfunction in endothelial cells through promoting lipid peroxidation: the protective role of autophagy, Am. J. Physiol. Heart Circ. Physiol. 302 (2012) H1394–H1409.
[12] A. Gaggar, R.P. Patel, There is blood in the water: hemolysis, hemoglobin, and heme in acute lung injury, Am. J. Physiol. Lung Cell Mol. Physiol. (2016) ajplung 00312 02016.
[13] H.B. Suliman, M.S. Carraway, L.W. Velsor, B.J. Day, A.J. Ghio, C.A. Piantadosi, Rapid mtDNA deletion by oxidants in rat liver mitochondria after hemin exposure,

Free Radic. Biol. Med. 32 (2002) 246–256.
[14] G.B. Fortes, L.S. Alves, R. de Oliveira, F.F. Dutra, D. Rodrigues, P.L. Fernandez, T. Souto-Padron, M.J. De Rosa, M. Kelliher, D. Golenbock, F.K. Chan, M.T. Bozza, Heme induces programmed necrosis on macrophages through autocrine TNF and ROS production, Blood 119 (2012) 2368–2375.
[15] J. Balla, G.M. Vercellotti, V. Jeney, A. Yachie, Z. Varga, H.S. Jacob, J.W. Eaton, G. Balla, Heme, heme oxygenase, and ferritin: how the vascular endothelium survives (and dies) in an iron-rich environment, Antioxidants Redox Signal. 9 (2007) 2119–2137.
[16] K. Heide, H. Haupt, K. Stoeriko, H.E. Schultze, On the heme-binding capacity of hemopexin, Clin. Chim. Acta 10 (1964) 460–469.
[17] J. Killander, Separation of human heme- and hemoglobin-binding plasma proteins, ceruloplasmin and albumin by gel filtration, Biochim. Biophys. Acta 93 (1964) 1–14.
[18] Y.I. Miller, A. Smith, W.T. Morgan, N. Shaklai, Role of hemopexin in protection of low-density lipoprotein against hemoglobin-induced oxidation, Biochemistry 35 (1996) 13112–13117.
[19] R.L. Nagel, Q.H. Gibson, The binding of hemoglobin to haptoglobin and its relation to subunit dissociation of hemoglobin, J. Biol. Chem. 246 (1971) 69–73.
[20] C.M. Shaver, C.P. Upchurch, D.R. Janz, B.S. Grove, N.D. Putz, N.E. Wickersham, S.I. Dikalov, L.B. Ware, J.A. Bastarache, Cell-free hemoglobin: a novel mediator of acute lung injury, Am. J. Physiol. Lung Cell Mol. Physiol. 310 (2016) L532–L541.
[21] S. Matalon, Mechanisms and regulation of ion transport in adult mammalian alveolar type II pneumocytes, Am. J. Physiol. 261 (1991) C727–C738.
[22] L.B. Ware, M.A. Matthay, Alveolar fluid clearance is impaired in the majority of patients with acute lung injury and the acute respiratory distress syndrome, Am. J. Respir. Crit. Care Med. 163 (2001) 1376–1383.
[23] M.L. Vivona, M. Matthay, M.B. Chabaud, G. Friedlander, C. Clerici, Hypoxia reduces alveolar epithelial sodium and fluid transport in rats: reversal by beta-adrenergic agonist treatment, Am. J. Respir. Cell Mol. Biol. 25 (2001) 554–561.
[24] P. Gwozdzinska, B.A. Buchbinder, K. Mayer, S. Herold, R.E. Morty, W. Seeger, I. Vadasz, Hypercapnia impairs ENaC cell surface stability by promoting phosphorylation, polyubiquitination and endocytosis of beta-ENaC in a human alveolar epithelial cell line, Front. Immunol. 8 (2017) 591.
[25] A. Lam, N. Vetal, S. Matalon, S. Aggarwal, Role of heme in bromine-induced lung injury, Ann. N. Y. Acad. Sci. 1374 (2016) 105–110.
[26] D.A. Ford, J. Honavar, C.J. Albert, M.A. Duerr, J.Y. Oh, S. Doran, S. Matalon, R.P. Patel, Formation of chlorinated lipids post-chlorine gas exposure, J. Lipid Res. 57 (2016) 1529–1540.
[27] A. Lazrak, J. Creighton, Z. Yu, S. Komarova, S.F. Doran, S. Aggarwal, C.W. Emala, V.P. Stober, C.S. Trempus, S. Garantziotis, S. Matalon, Hyaluronan mediates airway hyperresponsiveness in oxidative lung injury, Am. J. Physiol. Lung Cell Mol. Physiol. 308 (2015) L891–L903.
[28] N.J. Meyer, J.P. Reilly, R. Feng, J.D. Christie, S.L. Hazen, C.J. Albert, J.D. Franke, C.L. Hartman, J. McHowat, D.A. Ford, Myeloperoxidase-derived 2-chlorofatty acids contribute to human sepsis mortality via acute respiratory distress syndrome, JCI Insight **2** (2017).
[29] C.J. Albert, A.K. Thukkani, R.M. Heuertz, A. Slungaard, S.L. Hazen, D.A. Ford, Eosinophil peroxidase-derived reactive brominating species target the vinyl ether bond of plasmalogens generating a novel chemoattractant, alpha-bromo fatty aldehyde, J. Biol. Chem. 278 (2003) 8942–8950.
[30] B.K. Wacker, C.J. Albert, B.A. Ford, D.A. Ford, Strategies for the analysis of chlorinated lipids in biological systems, Free Radic. Biol. Med. 59 (2013) 92–99.
[31] M.A. Duerr, R. Aurora, D.A. Ford, Identification of glutathione adducts of alpha-chlorofatty aldehydes produced in activated neutrophils, J. Lipid Res. 56 (2015) 1014–1024.
[32] D. Pan, O. Vargas-Morales, B. Zern, A.C. Anselmo, V. Gupta, M. Zakrewsky, S. Mitragotri, V. Muzykantov, The effect of polymeric nanoparticles on biocompatibility of carrier red blood cells, PloS One 11 (2016) e0152074.
[33] A. Lazrak, A. Jurkuvenaite, L. Chen, K.M. Keeling, J.F. Collawn, D.M. Bedwell, S. Matalon, Enhancement of alveolar epithelial sodium channel activity with decreased cystic fibrosis transmembrane conductance regulator expression in mouse lung, Am. J. Physiol. Lung Cell Mol. Physiol. 301 (2011) L557–L567.
[34] A. Lazrak, K.E. Iles, G. Liu, D.L. Noah, J.W. Noah, S. Matalon, Influenza virus M2 protein inhibits epithelial sodium channels by increasing reactive oxygen species, Faseb. J. : Official Publication of the Federation of American Societies for Experimental Biology 23 (2009) 3829–3842.
[35] A. Lazrak, I. Nita, D. Subramaniyam, S. Wei, W. Song, H.L. Ji, S. Janciauskiene, S. Matalon, Alpha(1)-antitrypsin inhibits epithelial Na+ transport in vitro and in vivo, Am. J. Respir. Cell Mol. Biol. 41 (2009) 261–270.
[36] A. Keller, A.I. Nesvizhskii, E. Kolker, R. Aebersold, Empirical statistical model to estimate the accuracy of peptide identifications made by MS/MS and database search, Anal. Chem. 74 (2002) 5383–5392.
[37] A.I. Nesvizhskii, A. Keller, E. Kolker, R. Aebersold, A statistical model for identifying proteins by tandem mass spectrometry, Anal. Chem. 75 (2003) 4646–4658.
[38] D.B. Weatherly, J.A. Atwood 3rd, T.A. Minning, C. Cavola, R.L. Tarleton, R. Orlando, A Heuristic method for assigning a false-discovery rate for protein identifications from Mascot database search results, Mol. Cell. Proteomics : MCP 4 (2005) 762–772.
[39] S.A. Beausoleil, J. Villen, S.A. Gerber, J. Rush, S.P. Gygi, A probability-based approach for high-throughput protein phosphorylation analysis and site localization, Nat. Biotechnol. 24 (2006) 1285–1292.
[40] E. Krieger, G. Koraimann, G. Vriend, Increasing the precision of comparative models with YASARA NOVA–a self-parameterizing force field, Proteins 47 (2002) 393–402.
[41] S. Aggarwal, C.M. Gross, R. Rafikov, S. Kumar, J.R. Fineman, B. Ludewig, D. Jonigk, S.M. Black, Nitration of tyrosine 247 inhibits protein kinase G-1alpha activity by attenuating cyclic guanosine monophosphate binding, J. Biol. Chem. 289 (2014) 7948–7961.
[42] S. Noreng, A. Bharadwaj, R. Posert, C. Yoshioka, I. Baconguis, Structure of the human epithelial sodium channel by cryo-electron microscopy, eLife **7** (2018).
[43] Y. Duan, C. Wu, S. Chowdhury, M.C. Lee, G. Xiong, W. Zhang, R. Yang, P. Cieplak, R. Luo, T. Lee, J. Caldwell, J. Wang, P. Kollman, A point-charge force field for molecular mechanics simulations of proteins based on condensed-phase quantum mechanical calculations, J. Comput. Chem. 24 (2003) 1999–2012.
[44] M.A. Duerr, E.N.D. Palladino, C.L. Hartman, J.A. Lambert, J.D. Franke, C.J. Albert, S. Matalon, R.P. Patel, A. Slungaard, D.A. Ford, Bromofatty aldehyde derived from bromine exposure and myeloperoxidase and eosinophil peroxidase modify GSH and protein, J. Lipid Res. 59 (2018) 696–705.
[45] M.I. Hollenhorst, K. Richter, M. Fronius, Ion transport by pulmonary epithelia, J. Biomed. Biotechnol. (2011) 174306 2011.
[46] L. Chen, R.P. Patel, X. Teng, C.A. Bosworth, J.R. Lancaster Jr., S. Matalon, Mechanisms of cystic fibrosis transmembrane conductance regulator activation by S-nitrosoglutathione, J. Biol. Chem. 281 (2006) 9190–9199.
[47] Y. Guo, M.D. DuVall, J.P. Crow, S. Matalon, Nitric oxide inhibits Na+ absorption across cultured alveolar type II monolayers, Am. J. Physiol. 274 (1998) L369–L377.
[48] A. Lazrak, L. Chen, A. Jurkuvenaite, S.F. Doran, G. Liu, Q. Li, J.R. Lancaster Jr., S. Matalon, Regulation of alveolar epithelial Na+ channels by ERK1/2 in chlorine-breathing mice, Am. J. Respir. Cell Mol. Biol. 46 (2012) 342–354.
[49] J.R. Delanghe, M.R. Langlois, Hemopexin: a review of biological aspects and the role in laboratory medicine, Clin. Chim. Acta. Int. J. Clin. Chem. 312 (2001) 13–23.
[50] M.A. Gessner, S.F. Doran, Z. Yu, C.W. Dunaway, S. Matalon, C. Steele, Chlorine gas exposure increases susceptibility to invasive lung fungal infection, Am. J. Physiol. Lung Cell Mol. Physiol. 304 (2013) L765–L773.
[51] J. Honavar, S. Doran, K. Ricart, S. Matalon, R.P. Patel, Nitrite therapy prevents chlorine gas toxicity in rabbits, Toxicol. Lett. 271 (2017) 20–25.
[52] F.A. Wagener, A. Eggert, O.C. Boerman, W.J. Oyen, A. Verhofstad, N.G. Abraham, G. Adema, Y. van Kooyk, T. de Witte, C.G. Figdor, Heme is a potent inducer of inflammation in mice and is counteracted by heme oxygenase, Blood 98 (2001) 1802–1811.
[53] U. Muller-Eberhard, M. Fraig, Bioactivity of heme and its containment, Am. J. Hematol. 42 (1993) 59–62.
[54] C.D. Reiter, X. Wang, J.E. Tanus-Santos, N. Hogg, R.O. Cannon 3rd, A.N. Schechter, M.T. Gladwin, Cell-free hemoglobin limits nitric oxide bioavailability in sickle-cell disease, Nat. Med. 8 (2002) 1383–1389.
[55] G.L. Squadrito, E.M. Postlethwait, S. Matalon, Elucidating mechanisms of chlorine toxicity: reaction kinetics, thermodynamics, and physiological implications, Am. J. Physiol. Lung Cell Mol. Physiol. 299 (2010) L289–L300.
[56] A.C. Chou, C.D. Fitch, Mechanism of hemolysis induced by ferriprotoporphyrin IX, J. Clin. Investig. 68 (1981) 672–677.
[57] I. Kirschner-Zilber, E. Rabizadeh, N. Shaklai, The interaction of hemin and bilirubin with the human red cell membrane, Biochim. Biophys. Acta 690 (1982) 20–30.
[58] S.C. Liu, S. Zhai, J. Lawler, J. Palek, Hemin-mediated dissociation of erythrocyte membrane skeletal proteins, J. Biol. Chem. 260 (1985) 12234–12239.
[59] I. Solar, J. Dulitzky, N. Shaklai, Hemin-promoted peroxidation of red cell cytoskeletal proteins, Arch. Biochem. Biophys. 283 (1990) 81–89.
[60] Z. Szweda-Lewandowska, A. Krokosz, M. Gonciarz, W. Zajeczkowska, M. Puchala, Damage to human erythrocytes by radiation-generated HO* radicals: molecular changes in erythrocyte membranes, Free Radic. Res. 37 (2003) 1137–1143.
[61] M.A. Matthay, H.G. Folkesson, C. Clerici, Lung epithelial fluid transport and the resolution of pulmonary edema, Physiol. Rev. 82 (2002) 569–600.
[62] G.M. Mutlu, J.I. Sznajder, Mechanisms of pulmonary edema clearance, Am. J. Physiol. Lung Cell Mol. Physiol. 289 (2005) L685–L695.
[63] S. Matalon, H. O'Brodovich, Sodium channels in alveolar epithelial cells: molecular characterization, biophysical properties, and physiological significance, Annu. Rev. Physiol. 61 (1999) 627–661.
[64] E. Hummler, P. Barker, J. Gatzy, F. Beermann, C. Verdumo, A. Schmidt, R. Boucher, B.C. Rossier, Early death due to defective neonatal lung liquid clearance in alpha-ENaC-deficient mice, Nat. Genet. 12 (1996) 325–328.
[65] U. Thome, L. Chen, P. Factor, V. Dumasius, B. Freeman, J.I. Sznajder, S. Matalon, Na,K-ATPase gene transfer mitigates an oxidant-induced decrease of active sodium transport in rat fetal ATII cells, Am. J. Respir. Cell Mol. Biol. 24 (2001) 245–252.
[66] J.D. Brand, A. Lazrak, J.E. Trombley, R.J. Shei, A.T. Adewale, J.L. Tipper, Z. Yu, A.R. Ashtekar, S.M. Rowe, S. Matalon, K.S. Harrod, Influenza-mediated reduction of lung epithelial ion channel activity leads to dysregulated pulmonary fluid homeostasis, JCI Insight **3** (2018).
[67] P.L. Brazee, L. Morales-Nebreda, N.D. Magnani, J.G. Garcia, A.V. Misharin, K.M. Ridge, G.R.S. Budinger, K. Iwai, L.A. Dada, J.I. Sznajder, Linear ubiquitin assembly complex regulates lung epithelial driven responses during influenza infection, J. Clin. Investig. (2019).
[68] P. Factor, F. Saldias, K. Ridge, V. Dumasius, J. Zabner, H.A. Jaffe, G. Blanco, M. Barnard, R. Mercer, R. Perrin, J.I. Sznajder, Augmentation of lung liquid clearance via adenovirus-mediated transfer of a Na,K-ATPase beta1 subunit gene, J. Clin. Investig. 102 (1998) 1421–1430.
[69] C. Peteranderl, L. Morales-Nebreda, B. Selvakumar, E. Lecuona, I. Vadasz, R.E. Morty, C. Schmoldt, J. Bespalowa, T. Wolff, S. Pleschka, K. Mayer, S. Gattenloehner, L. Fink, J. Lohmeyer, W. Seeger, J.I. Sznajder, G.M. Mutlu, G.R. Budinger, S. Herold, Macrophage-epithelial paracrine crosstalk inhibits lung edema clearance during influenza infection, J. Clin. Investig. 126 (2016) 1566–1580.
[70] H.L. Ji, X.F. Su, S. Kedar, J. Li, P. Barbry, P.R. Smith, S. Matalon, D.J. Benos, Delta-subunit confers novel biophysical features to alpha beta gamma-human epithelial

sodium channel (ENaC) via a physical interaction, J. Biol. Chem. 281 (2006) 8233–8241.
[71] G. Otulakowski, B. Rafii, H. O'Brodovich, Differential translational efficiency of ENaC subunits during lung development, Am. J. Respir. Cell Mol. Biol. 30 (2004) 862–870.
[72] G. Frindt, Z. Ergonul, L.G. Palmer, Na channel expression and activity in the medullary collecting duct of rat kidney, Am. J. Physiol. Ren. Physiol. 292 (2007) F1190–F1196.
[73] Ismailov II, B.K. Berdiev, D.J. Benos, Biochemical status of renal epithelial Na+ channels determines apparent channel conductance, ion selectivity, and amiloride sensitivity, Biophys. J. 69 (1995) 1789–1800.
[74] M.B. Butterworth, R.S. Edinger, R.A. Frizzell, J.P. Johnson, Regulation of the epithelial sodium channel by membrane trafficking, Am. J. Physiol. Ren. Physiol. 296 (2009) F10–F24.
[75] M.B. Butterworth, R.S. Edinger, J.P. Johnson, R.A. Frizzell, Acute ENaC stimulation by cAMP in a kidney cell line is mediated by exocytic insertion from a recycling channel pool, J. Gen. Physiol. 125 (2005) 81–101.
[76] M.B. Butterworth, S.I. Helman, W.J. Els, cAMP-sensitive endocytic trafficking in A6 epithelia, Am. J. Physiol. Cell Physiol. 280 (2001) C752–C762.
[77] S. Wang, S. Publicover, Y. Gu, An oxygen-sensitive mechanism in regulation of epithelial sodium channel, Proc. Natl. Acad. Sci. U.S.A. 106 (2009) 2957–2962.
[78] X.D. Tang, R. Xu, M.F. Reynolds, M.L. Garcia, S.H. Heinemann, T. Hoshi, Haem can bind to and inhibit mammalian calcium-dependent Slo1 BK channels, Nature 425 (2003) 531–535.
[79] W. Song, S. Wei, Y. Zhou, A. Lazrak, G. Liu, J.D. Londino, G.L. Squadrito, S. Matalon, Inhibition of lung fluid clearance and epithelial Na+ channels by chlorine, hypochlorous acid, and chloramines, J. Biol. Chem. 285 (2010) 9716–9728.